

Green Chemistry

Accepted Manuscript



This is an *Accepted Manuscript*, which has been through the Royal Society of Chemistry peer review process and has been accepted for publication.

Accepted Manuscripts are published online shortly after acceptance, before technical editing, formatting and proof reading. Using this free service, authors can make their results available to the community, in citable form, before we publish the edited article. We will replace this *Accepted Manuscript* with the edited and formatted *Advance Article* as soon as it is available.

You can find more information about *Accepted Manuscripts* in the [Information for Authors](#).

Please note that technical editing may introduce minor changes to the text and/or graphics, which may alter content. The journal's standard [Terms & Conditions](#) and the [Ethical guidelines](#) still apply. In no event shall the Royal Society of Chemistry be held responsible for any errors or omissions in this *Accepted Manuscript* or any consequences arising from the use of any information it contains.



www.rsc.org/greenchem



Green Chemistry

ARTICLE

Facile extraction of cellulose nanocrystals from wood using ethanol and peroxide solvothermal pretreatment followed by ultrasonic nanofibrillation †

Received 00th September 2015,
Accepted 00th January 20xx

DOI: 10.1039/x0xx00000x

www.rsc.org/greenchem

Yanna Li, Yongzhuang Liu, Wenshuai Chen, Qingwen Wang, Yixing Liu, Jian Li and Haipeng Yu*

Cellulose nanocrystals (CNCs) were successfully extracted from wood flour by a two-step process that comprised ethanol and peroxide solvothermal pretreatment and an ultrasonic disintegration process. Characterization results showed that 97% of the total lignin and 70% of the hemicellulose could be fractionated in a single ethanosolv pretreatment step. Additional treatment with alkaline hydrogen peroxide removed the residual lignin and hemicellulose and resulted in high purity cellulose. The CNCs obtained after ultrasonication displayed a similar yield, size, morphology, and crystallinity but had better thermal stability and film forming properties than those produced by concentrated acid hydrolysis. Overall, the solvothermal treatment using ethanol and its combination with peroxide is an ideal substitute method for pretreatment of lignocellulose. Further integration of such pretreatments with ultrasonication provides a promising efficient process with low environmental impact for production of CNCs.

Introduction

The current global focus on biomass refinery of lignocellulose is not only limited to the production of liquid fuels and chemicals but also includes intermediate products such as nanocellulose.^{1,2} As a kind of polysaccharide nanosized material that can be extracted from natural lignocellulosic biomass, nanocellulose displays exceptional properties such as low density, high specific strength and modulus, large surface area, and reactive surfaces.³ Thanks to its distinctive properties, nanocellulose has been found to be versatile and useful in a variety of applications such as a reinforcing filler, rheological modifier, pharmaceutical carrier, biomedical implant, and as a substrate of electronic components.^{4–8} However, nanocellulose is embedded in the plant cell walls that have hierarchical structures and complex compositions. The strong outermost lignin layers and inner cemented hemicellulose are major obstacles for direct access to the nanocellulose.³ In addition, extensive cross-links exist between cellulose and lignin as well as hemicellulose through ester and ether linkages. All the above factors synthetically result in the hydrolytic stability and structural robustness of lignocellulose; the related phenomenon is also called biomass recalcitrance (resistance of cell walls to deconstruction).

Several processes have been used to extract nanocellulose from lignocellulose. These methods include chemical treatments, e.g., acid hydrolysis, TEMPO-mediated oxidation hydrolysis treatment; mechanical treatments, e.g., cryocrushing, grinding, high-pressure

homogenization, high-intensity ultrasonication, and twin-screw extrusion; biological treatments, e.g., enzyme-assisted hydrolysis; as well as a combination of two or several of the aforementioned methods. All these methods lead to different types of nanocelluloses, depending on the pretreatment of the raw material, and more importantly, on the disintegration process itself.⁹ Among the various methods for fabrication of nanocellulose, the pretreatment process for the removal of lignin and hemicellulose is mandatory to overcome the recalcitrance and facilitate the subsequent processing.^{9–11} The delignification/fractionation of lignocellulose using sulfite, chlorite, diluted-acid, or alkaline solution was very common, however, the process was usually tedious and to some degree detrimental to the environment.¹² Toward the manufacture at an industrial scale, nanocellulose needs to be extracted in high yield with minimal steps and in an environmentally friendly manner. To increase the technical and economic feasibility, it is very important to obtain high purity cellulose with less constraints. Nowadays, biomass refinery methods are receiving great attention, in light of their advantages in fractionation/delignification of lignocellulosic biomass. The biorefinery processes can ensure the deconstruction of noncellulosic polymeric compositions in lignocellulose, while maintaining the cellulose part for further disintegration into nanocellulose. Among the new type of pretreatment protocols, organosolv treatment results in an efficient fractionation of lignocellulose into its main components, thus allowing the valuable conversion into useful end products.^{13–17} Historically, organosolv treatment has been investigated primarily for pulp-making, but nowadays it is receiving attention as an important pretreatment method for biomass refinery.^{13,18} Organic solvents act as dissolving agents by solubilizing lignin and some of hemicellulose under heating conditions and leaving relatively pure cellulose residues. A

Key Laboratory of Bio-based Material Science and Technology, Ministry of Education, Northeast Forestry University, Harbin 150040, China.
E-mail: yuhaipeng20000@gmail.com

† Electronic Supplementary Information (ESI) available: See DOI: 10.1039/x0xx00000x

variety of organic solvents including alcohols, acids, esters, ketones, phenols, and amines, provide many choices for targeted treatment of biomass. Solvents with low boiling points (e.g., ethanol) are the major solvents used because of their low cost and solubility in water.^{19, 20} Another advantage is the ease of recovery by simple distillation, which requires low energy consumption.^{21–23} The OH⁻ ion from the ethanol solvent will attack the acid-ester bonds of lignin–hemicellulose compounds. The cleavage of ether linkages in lignin and partial hydrolysis of the glycosidic bonds in hemicellulose are also important for the breakdown of aromatics and polysaccharides of lignocellulose. Usually, mineral acid (e.g., sulfuric acid), organic acid (e.g., formic acid and acetic acid), organic peroxide (such as hydrogen peroxide), alkali, and salt (e.g., magnesium chloride) are added to catalyze the delignification process and hemicellulose hydrolysis.^{16, 17, 22–24}

In light of the prominence of using ethanol and peroxide in delignification/fractionation of lignocellulosic biomass, they are the suitable choices as the pretreatment solvents in this study. It is conceived that the integration of ethanol and peroxide pretreatment with ultrasonic processing will contribute to efficient fabrication of nanocellulose free of environmental pollution. By modulating the solvent and reaction conditions, utmost fractionation and removal of the noncellulosic compositions is expected, and pure cellulose to be retained for nanocellulose fabrication. This study mainly focused on the pretreatment effects of these solvents, as well as their impact on the subsequent ultrasonic disintegration process into nanocellulose. The pretreatment efficacy was evaluated by chemical component analysis and combinational spectroscopy techniques. The properties of the resultant nanocellulose in terms of structure, morphology, crystallinity, thermal degradation, and its fabrication into nanofilms were comprehensively investigated.

Experimental

Materials

Wood (*Populus ussuriensis*) flour sieved under 60-mesh was selected as a lignocellulosic feedstock. Ethanol, sulfuric acid (H₂SO₄), sodium hydroxide (NaOH) and hydrogen peroxide (H₂O₂) were all of analytical grade and purchased from Tianjin Kermel Chemical Reagent Co., Ltd.

Ethanol solvothermal treatment

Ethanol solvothermal experiment was carried out in a chemical reactor comprising a sleeve and a polytetrafluoroethylene cylinder liner. An ethanol/water mixture (65:35 v/v) was used as reaction medium, and a 0.07 mol L⁻¹ H₂SO₄ solution as catalyst. The solid/liquid ratio of wood flour to solvent was 1:9 (w/v). The reactor was heated at a heating rate of 10 °C min⁻¹ to the set point temperature (165, 180, or 195 °C), and then was left to proceed isothermally for 80 min. The insoluble residues were filtered and washed using the same aqueous ethanol for three times to prevent re-depositing lignin. For convenience, the solid residues correspondingly obtained at reaction temperature 165 °C, 180 °C and 195 °C were labeled as OP165, OP180, and OP195, respectively. The liquid fractions were concentrated by rotary evaporation at 50

°C under reduced pressure, and poured into water to precipitate the dissolved lignin, and labeled as OL165, OL180, and OL195.

Alkaline hydrogen peroxide treatment

The OP180 was selected for further bleaching treatment with a mixture solution containing 5 wt% H₂O₂ and 4 wt% NaOH. The solid/liquid ratio was 1:20 (w/v). The reaction experiment was performed in a beaker at 50 °C for 90 min. After the peroxide treatment, a cream-like slurry was obtained and named as BOP180.

Ultrasonic nanofibrillation

The OP165, OP180, OP195 and BOP180 samples were soaked in distilled water (concentration: 0.5 wt%, calculated by weight percentage of oven-dried sample to solution). Then the solutions were placed in an ultrasonic generator (JY99-IIDN, Ningbo Scientz Biotechnology Co., Ltd., China) equipped with a cylindrical titanium alloy probe (25 mm in diameter). The ultrasonication with a frequency of 20 kHz was conducted at output power 1200 W for 20 min, resulting in the cellulose nanocrystals (CNCs) that labeled as OPU165, OPU180, OPU195 and BOPU180, respectively. The yield of them was calculated as the weight percentage of oven-dried CNCs to the oven-dried wood feedstock.

Preparation of CNC nanofilms

Each 5 mL of 0.5 wt% suspension of OPU165, OPU180, OPU195 and BOPU180 was filtrated using a filter membrane (pore size: 0.45 μm, Xinya Purification Devices Co. Ltd., Shanghai, China). Then, the obtained wet gel sheets were sandwiched between two filter membranes, and oven dried at 60 °C for 12 h to achieve thin films.

Characterization

Chemical composition analysis. The chemical composition of the raw wood flour and the obtained samples was determined as previously described,²⁵ and expressed as wt% content of Klason lignin, hemicellulose, and α-cellulose. A minimum of three times testing on each sample was performed, and their averaged value was calculated.

Fourier transform infrared (FT-IR) spectroscopy. FT-IR spectra were measured using a Nicolet Magna 560 FT-IR instrument (Thermo Fisher Corp., USA). The spectra were measured in ATR mode, and data recorded over the range from 650 to 4000 cm⁻¹, with a resolution of 4 cm⁻¹.

¹H–¹³C correlation two-dimensional heteronuclear single quantum coherence (2D–HSQC) nuclear magnetic resonance (NMR) spectroscopy. The liquid fraction OL180 (90 mg) were dissolved in 0.5 mL deuterated dimethyl sulfoxide (DMSO-d₆). The 2D–HSQC NMR spectra were acquired on an Agilent Pro Pulse 500MHz spectrometer, and recorded in the gradient HSQC adiabatic version. The spectral widths were 20000 and 5000 Hz for the ¹³C and ¹H dimensions, respectively. The number of collected complex points was 1024 for the ¹H dimension with a recycle delay of 1.5 s, the number of transients was 128, and 256 time increments were recorded in the ¹³C dimension. Prior to Fourier transformation, the data matrices were zero filled to 1024 points in the ¹³C dimension.

Green Chemistry ARTICLE

Gel permeation chromatography (GPC) analysis. Molecular weights of the lignin fractions were measured by WATERS 2695 GPC with a signal detector of differential refractive index detector (WATERS 2414). The column was operated at ambient temperature and eluted at a flow rate of 1 mL min^{-1} .

^{13}C cross-polarization/magic angle spinning (CP/MAS) NMR spectroscopy. The ^{13}C CP/MAS NMR analysis on the pretreated residues was carried out at room temperature with a BRUKER DRX-400 instrument. Spectra were acquired with a 4-mm magic angle sample spinning (MAS) probe, using a combination of cross-polarisation (CP), MAS and high-power proton decoupling methods. A total of 800 scans were accumulated for each sample.

UV-vis spectroscopy. The UV-vis spectroscopy of aqueous CNC suspensions were tested in the wavelength range of 300–800 nm by a TU-1900 spectrophotometer (Beijing Purkinje General Instrument Co. Ltd, China). The light transmittance spectra of CNC nanofilms were recorded using a TU-1901 spectrophotometer (Beijing Purkinje General Instrument Co. Ltd, China). The scanning wavelength range was from 200 nm to 800 nm.

Zeta potential (ZP) analysis. Surface charge of the obtained CNCs in suspension was measured using dynamic light scattering with a zetasizer (Nano ZS, Malvern, UK).

Transmission electron microscopy (TEM) observation. TEM observation on the resultant CNCs was performed using a FEI Tecnai G2 microscope at an accelerate voltage 80 kV. A droplet ($5 \mu\text{L}$) of diluted slurry was dropped on the carbon-coated electron microscopy grid, and then was negatively stained by 1 wt% phosphotungstic acid solution to enhance the contrast of image. The sizes of CNCs were measured from the TEM images using an image analysis system (TDY-V5.2, Beijing Tianhong Precision Instrument Technology Co. Ltd., China).

X-ray diffraction (XRD) analysis. The XRD patterns were obtained using an X-ray diffractometer (D/max 2200, Rigaku, Japan) with Ni-filtered $\text{Cu K}\alpha$ radiation ($\lambda = 0.154 \text{ nm}$) at 40 kV and 30 mA. The diffraction data were collected from $2\theta = 5\text{--}40^\circ$ at a scanning rate of 4° min^{-1} . The relative crystallinity index (Crl) was estimated using the Segal method²⁶ by following the equation:

$$\text{Crl}(\%) = \frac{I_{200} - I_{\text{am}}}{I_{200}} \times 100$$

where I_{200} is the peak intensity of the (002) lattice diffraction at $2\theta \approx 22.6^\circ$, which represents both the crystalline and amorphous region material, and I_{am} is the diffraction intensity of amorphous fraction at $2\theta \approx 18^\circ$.

Thermogravimetric (TG) analysis. The TG analysis on the samples was performed using a TG analyzer (Pyris 6, PerkinElmer, USA) at a heating rate of $10^\circ \text{C min}^{-1}$ in nitrogen atmosphere.

Scanning electron microscopy (SEM) observation. The microstructures of the obtained nanofilms were observed using a field emission scanning electron microscope (Sirion 200, FEI, Netherlands) at low acceleration voltages (10–15 kV). Before observation the samples were coated with platinum using a vacuum sputter coater.

Mechanical testing. Tensile tests on the nanofilms were performed at room temperature using an Instron 5569 universal testing machine at a cross-head speed of 1 mm min^{-1} . The dimensions of the test specimens were $10 \text{ mm} \times 5 \text{ mm} \times 0.02\text{--}0.03 \text{ mm}$.

Results and discussion

Chemical composition analysis

The aim of the ethanol and peroxide pretreatment is delignification of lignocellulose and removal of noncellulosic components. The effect of the pretreatment was first characterized by chemical composition analysis (Table 1). In the raw wood feedstock, the α -cellulose, hemicellulose, and Klason lignin contents were 46.08%, 34.67%, and 19.09%, respectively. After the ethanol solvothermal pretreatment, about 97% of the total lignin and 70% of the hemicellulose were fractionated from the lignocellulose. The value of Klason lignin content reflects that of the solvothermal pretreatment using ethanol solvent, effectively generating a high content of carbohydrates. However, the Klason lignin and hemicellulose contents seem to vary with reaction temperature. The phenomenon is proposed to be caused by the increased degradation of hemicellulose and partial cellulose at 195°C compared with 180°C ; the Klason lignin content increased proportionally. The increase of hemicellulose content after treatment at 195°C was also perhaps as a result of degradation of partial amorphous cellulose. When a further peroxide treatment was applied, another one third of hemicellulose could be fractionated, and the remaining lignin almost disappeared. The reactivity of peroxide results from the generation of highly reactive superoxide radicals ($-\text{O}_2^-$), which are responsible for the oxidation of the aromatic rings of lignin and parts of hemicellulose to carboxylic acids compounds.^{27, 28} The peroxide was suitable for extraction of cellulose because the oxidation agent is more aggressive towards lignin and hemicellulose, whereas cellulose is hardly decomposed under the mild conditions.²⁷ Ultimately, the α -cellulose became the predominant component and accounted for 95 % of the remaining material.

Table 1. Chemical composition analysis of the pretreated samples

Sample	Klason lignin /%	hemicellulose /%	α -cellulose /%
wood	19.09 \pm 0.45	34.67 \pm 0.22	46.08 \pm 0.56
OP165	0.40 \pm 0.04	11.01 \pm 1.91	88.43 \pm 3.82
OP180	0.50 \pm 0.08	7.24 \pm 1.07	90.16 \pm 1.16
OP195	0.64 \pm 0.01	10.44 \pm 2.51	88.57 \pm 2.54
BOP180	0.10 \pm 0.10	4.91 \pm 0.22	93.18 \pm 0.22

Structural elucidation of the pretreated samples and fractions

The complete delignification of lignocellulose is a challenge because the lignin has strong poly-ring C–O–C and C–C bonds as well as lignin–carbohydrate bonds. FT-IR spectra of the pretreated samples (Fig. 1a) help to reveal the structural transformation. The absorbance peaks at 1593, 1505, and 1457 cm^{-1} , which are all found in spectra of wood, often represent the aromatic parts of lignin. The peaks at 1593 and 1505 cm^{-1} represent aromatic skeletal vibrations and C=O stretching; the peak at 1457 cm^{-1} belongs to C–H deformations and asymmetry in $-\text{CH}_3$ and $-\text{CH}_2-$.²⁹ The disappearance of these bands was associated with lignin removal and hints that the pretreatment had produced a significant delignification effect. The decrease in the intensity of both prominent bands at 1732 and 1235 cm^{-1} (representing the carboxyl groups and attributed either to the acetyl and uronic ester groups

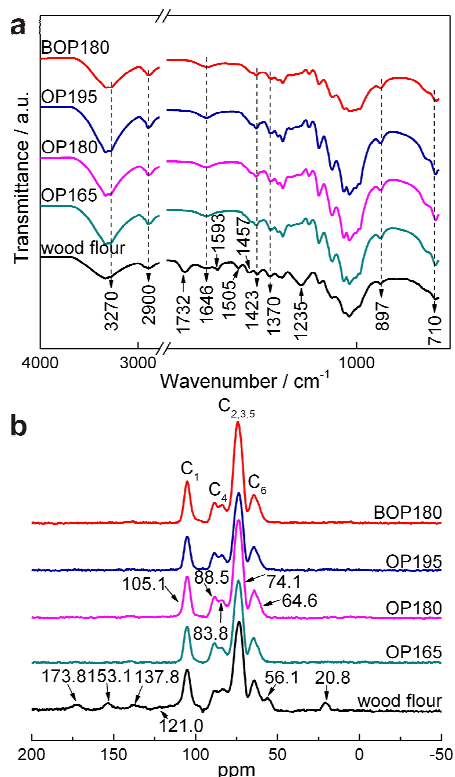


Fig. 1 (a) FT-IR spectra and (b) ¹³C CP/MAS NMR spectra of raw wood feedstock and the pretreated samples.

of the hemicellulose or to the ester linkage of the carboxyl groups of lignin and/or hemicellulose) indicated the dissolution/removal of hemicellulose. After the ethanol and peroxide pretreatments, all the above mentioned absorption peaks disappeared, while the characteristic absorption peak at 1646 cm⁻¹ enhanced, possibly corresponding to the presence of carboxyl and hemiacetal groups.

To further elucidate the structural transformation of lignocellulose and the breaking mode of the chemical bonds between lignin and the associated carbohydrates, 2D-HSQC NMR technique was used to characterize the samples. The lignin fractions of lignocellulose subjected to ethanol pretreatment at 180 °C was selected as representative. As shown in the HSQC spectrum of OL180 in Fig. 2, the side-chain regions (δ_C/δ_H 50–110/2.5–6.0 ppm) and aromatic regions (δ_C/δ_H 100–135/5.5–8.5 ppm) provided the main signals. The main cross-signals in the 2D-HSQC spectra were assigned according to the literature^{21,30,31} and are listed in Tables S1 and S2 of the ESI[†]. Firstly, we can see that there were no signals in the carbohydrates regions (δ_C/δ_H 91–105/3.9–5.4 ppm, dashed area in Fig. 2a), which are mainly assigned to the lignin–carbohydrate complex (LCC) structures.^{32,33} This reveals that during the delignification process, lignin–carbohydrate bonds were cleaved. Secondly, in the side-chain regions, except for the strong methoxy group signals (δ_C/δ_H 56.1/3.77 ppm), the signals of β -O-4' linkages (δ_C/δ_H 60.0/3.69 and 60.5/3.83 ppm) were also obvious, but the signals of β - β' were weak and those of β -5' could not even be detected. Furthermore, a semiquantitative method was used to identify the relative abundance of the three main structures in the

side-chain regions. C_v-H_v correlations were used to estimate the relative abundance to avoid possible interference from homonuclear ¹H-¹H couplings. In the aromatic regions, the syringyl/guaiacyl (S/G) ratio of lignin fractions was calculated according to C_{2,6}-H_{2,6} correlations from the S units and C₂-H₂ plus C₆-H₆ correlations from the G units. Most of the linkages were β -O-4' with a relative percentage of 99.46% and β - β' with a relative percentage of 0.54%. The relative percentage of β -O-4' linkages had an obvious improvement whereas the percentage of other linkages dropped.³⁴ From this result, the lignin fractions were apparently degraded during the solvothermal process, but we still need to confirm whether the β -O-4' structure was degraded. Thirdly, in the aromatic regions (Fig. 2b), the spectra indicate that the main unit structures of lignin fractions were syringyl and guaiacyl. The signals of S_{2/6} (δ_C/δ_H 103.8/6.64 ppm) and G₅ (δ_C/δ_H 115.4/6.81 ppm) were present before the pretreatment, but the signals of G₂ and G₆ disappeared after the treatment. This indicates that pretreatment may selectively degrade the G-type lignin or transform it to S-type or p-hydroxyphenyl-type lignin. Those parts of lignin might degrade into low molecular weight fragments and dissolve in ethanol.

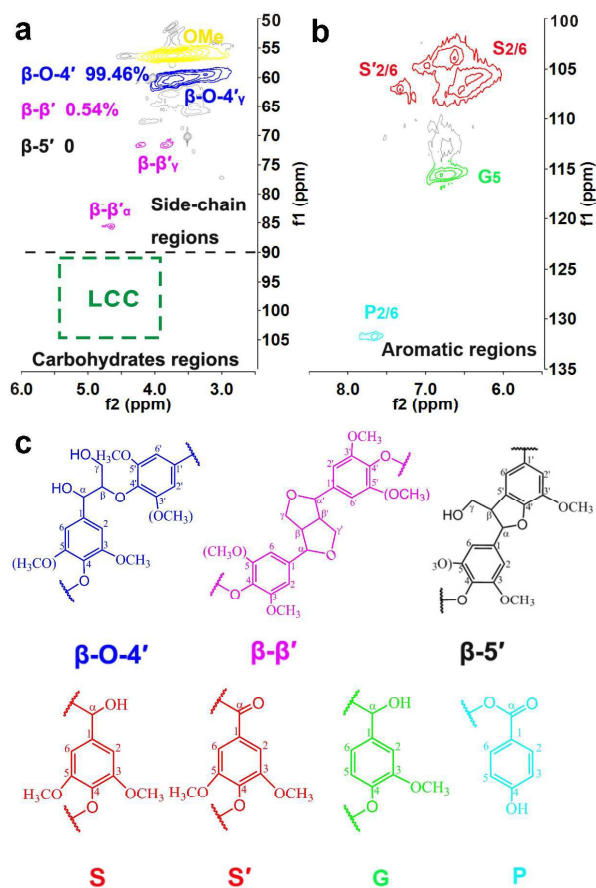


Fig. 2 2D-HSQC NMR spectra of the liquid fraction OL180: (a) side-chain regions (δ_C/δ_H 50–110/2.5–6.0) and (b) aromatic regions (δ_C/δ_H 100–135/5.5–8.5). (c) The relative structural linkages of lignin polymers are presented as references.

Green Chemistry ARTICLE

Table 2. M_w , number-average molecular weight (M_n) and polydispersity (M_w/M_n) of lignin fractions

Sample	M_w /g mol ⁻¹	M_n /g mol ⁻¹	M_w/M_n
OL165	2024	1401	1.44
OL180	1678	1278	1.31
OL195	1775	1272	1.40

To further verify the results, molecular weight was tested by GPC (Fig. S1 in ESI[†]). In comparison with the literatures,³⁵ the weight-average molecular weight (M_w) of the lignin fractions decreased to 1678–2024 g mol⁻¹, and a narrow molecular weight distribution (polydispersity = 1.31–1.44) was noted (Table 2). The low M_w and polydispersity suggest that the pretreatment could promote the depolymerization of oligomer intermediates to small molecules. According to the conjoint analysis of 2D-HSQC NMR and GPC, the main delignification routes of lignocellulose are concluded to be as follows: First, the LCC bonds of the aryl ethers and phenyl glycosides were cleaved, and lignin fractions with relatively large M_w were free in the system. Then, the free lignin fractions underwent the scission of C–C and C–O–C bonds to generate specific phenolic compounds with small M_w .²¹

Morphology and structure of cellulose fragments

After pretreatment, the insoluble cellulose fragments showed typical morphology similar to bleached pulp fibers (Fig. S2c–f in ESI[†]). They are considered consisting of millions of cellulose elementary fibrils and nanocrystals. For OP165 sample, a few unchangable cell wall fragments survived (Fig. S2c-inset), suggesting the inadequate reaction temperature for pretreatment. The homogeneity of fragments of OP180 and OP195 was better than that of OP165, revealing that the desired treatment temperature was 180 °C or above. The morphology of BOP180 was smoother than the others, indicating that the peroxide was conducive to the further fractionation of lignocellulose into refining pulp.

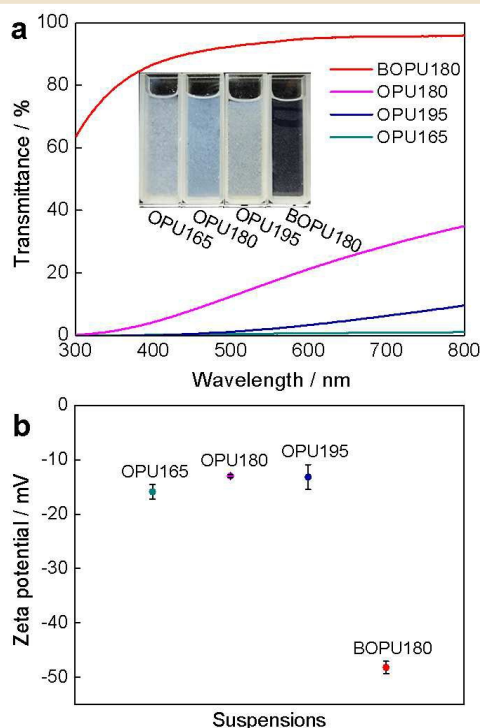
The cellulose fragments were further analyzed by FT-IR spectroscopy. In an FT-IR spectrum of raw wood feedstock, the absorbance peaks at 2900, 1423, 1370, 1160, 1115, 1060 and 897 cm⁻¹ are associated with the typical features of cellulose. The peak at 1423 cm⁻¹ corresponding to bending of –CH₂ groups can be assigned as the –C–6CH₂– of cellulose. The peak at 1370cm⁻¹ corresponds to the bending vibration of –CH and the stretching vibration of C–O.^{36,37} The presence of above mentioned peaks was in agreement with the cellulose structure (Fig. 1a). Furthermore, no apparent differences were observed in the spectra of cellulose fragments from different reaction temperatures.

The structural elucidation of cellulose fragments was performed using ¹³C CP/MAS NMR spectroscopy, as shown in Fig. 1b. The spectrum of the control sample (raw wood feedstock) represents a typical spectral pattern of lignocellulose. The noticeable signals between 110 ppm to 60 ppm are assigned to cellulose. The signals at 173.8 ppm and 20.8 ppm are attributed to the carbonyl carbons (–COO–, CH₃–COO–) and methyl carbons (CH₃–COO–) in acetyl group of hemicellulose, respectively.³⁸ The signals at 153.1 ppm (C₃ and C₅ in S-type units), 137.8 ppm (C₁ and C₄ in S-type units, C₁ in G-type units) and 56.1 ppm (OCH₃) are ascribed to lignin. A comparison between the spectra reveals that the characteristic signals of lignin and hemicellulose of the control sample

disappeared after pretreatment, while those assigned to cellulose remained and showed no remarkable changes.

Morphology and size distribution of the obtained CNCs

After pretreatment, the cellulose fragments were subjected to ultrasonic processing. The strong ultrasonic cavitation improved the degree of disintegration of cellulose fragments, and generated CNCs. A substantial change was observed in the dispersion of the CNCs in water (Fig. S3 in ESI[†]). All the CNC suspensions were stable and no precipitates were observed for over 6 months. This result suggested that the size of the CNCs was small enough to be well dispersed in aqueous solutions. The surface charge of the CNCs was detected by ZP measurements, which all showed a negative ZP (Fig. 3b). The OPU165, OPU180, and OPU195 samples showed small ZP values, which were close to those that undergo a short acid hydrolysis time, and smaller than those that undergo a long acid hydrolysis time.³⁹ Such ZP values were also lower than those of cellulose fibers produced by various pulping processes (between –20 mV and –45 mV).⁴⁰ Small ZP values suggested weak electrostatic repulsive forces among the CNC fibers. Thus, the CNC fibers are likely to aggregate together and give rise to the opaque appearance of a suspension (Fig. 3a). Interestingly, with the introduction of peroxide treatment, the amount of non-disintegrated aggregates almost disappeared, and the electrostatic repulsive forces among the CNC fibers significantly increased (–48 mV). Thus, the suspension of BOPU180 was especially transparent compared to the other suspensions, with the light transmittance of a 0.5 wt% suspension reaching 95.0% at 600 nm. We attribute this difference to the presence of more hydrophilic carbonyl groups or enol ethers resulting from the oxidation of some hydroxyl groups.

**Fig. 3** (a) UV-vis transmittance spectra of 0.5 wt% CNC suspensions. (b) Zeta potential plot of the CNC suspensions.

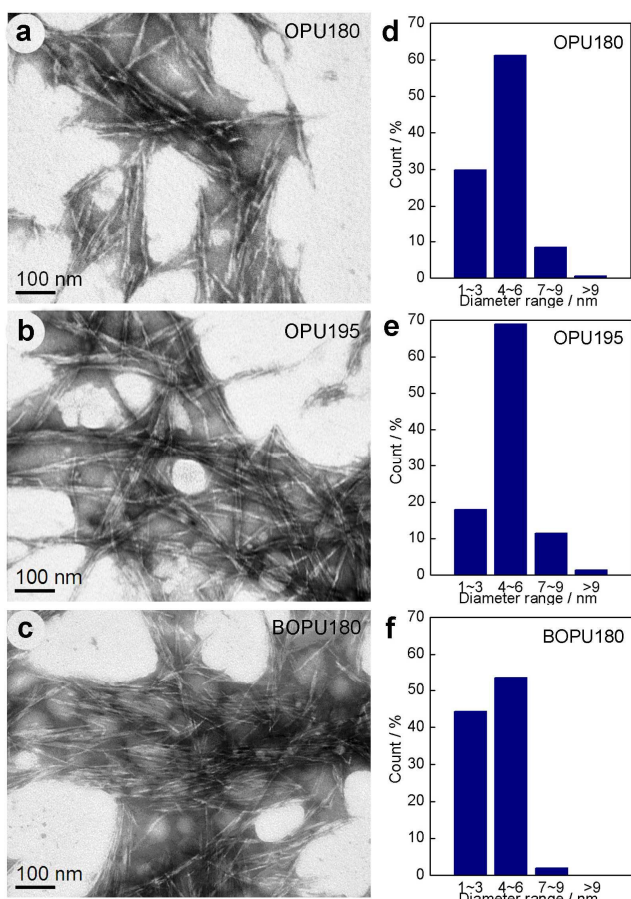


Fig. 4 TEM images show the (a–c) morphology and (d–f) size distribution of the resultant CNCs.

Morphology and size observation on the obtained CNCs was proceeded by TEM. Even though the same ultrasonic condition was conducted, different results of diameter size and morphology were received. The TEM image of OPU165 shows massive fibers with a diameter of 1–16 nm, but some micron-sized short fragments or aggregates were also present, indicating that the processing was not complete. This might be caused by the insufficient reaction temperature during ethanosolv pretreatment. Nanosized CNC fibers were clearly observed in the TEM images of OPU180, OPU195, and BOPU180 (Fig. 4). The widths ranged between 1–9 nm and the lengths were less than 500 nm, which are similar to those of CNCs obtained by sulfuric acid hydrolysis.^{39,40} The yield of OPU165 was 41.44%, and this comparatively high value might be caused by the existence of remanent hemicellulose and undissolved cytoderm fragments (Fig. S4, ESI†). The yield of OPU180, OPU195 and BOPU180 was 24.84%, 19.18% and 22.38%, respectively, equivalent to those produced by concentrated acid hydrolysis methods.⁴¹

Crystallinity and thermal stability of the obtained CNCs

With respect to the change of crystal structure and the crystallinity, the OP and OPU samples were analyzed using XRD. As seen in Fig. 5, all the XRD patterns exhibited the typical diffraction peaks around $2\theta=16^\circ$ and 22.6° , which confirmed that the crystal lattice type I of

native cellulose was preserved although it had gone through a series of treatments. The CrI, as a key factor in influencing the mechanical and thermal properties, was calculated according to the Segal method. The CrI of the ethanosolv pretreated samples was 79.37–84.37%, showing a 9–14% enhancement from the raw feedstock (70.72%). The increase in the CrI undoubtedly resulted from the removal of lignin and hemicellulose. The fact that the CrI of OP180 (84.37%) was higher than that of OP165 (79.37%) confirmed the preferred ethanosolv temperature of 180 °C. The CrI of OP180 was also higher than that of OP195 (80.41%), indicating that the excessive temperature of 195 °C might have a destructive effect on the amorphous region and imperfect crystalline region of cellulose. After ultrasonication, the type I crystal lattice of the obtained CNCs was unchanged (Fig. S5, ESI†), but the CrI values decreased by 2–10% compared to those of the corresponding OP samples. The CrI of BOP180 reached the highest value (86.59%), because of the apparent removal of lignin and hemicellulose.

TG and DTG (a derivative of TG, representing the corresponding rate of weight loss) curves are shown in Fig. 6. Compared with raw feedstock, the TG and DTG curves of the OP samples only displayed the loss of cellulose. The starting decomposition temperature occurred at 310 °C, and the maximum degradation rate appeared at around 340 °C. No obvious differences were found between the TG and DTG curves of OP and OPU samples. This implied that ultrasonic treatment had no negative effects on the thermal stability of the CNCs. The temperature corresponding to the maximum degradation rate of BOPU180 (355 °C) was higher than that of OPU180 (340 °C). Furthermore, the curve of BOPU180 showed an earlier weight loss that started at around 200 °C, displaying that peroxide treatment also had a negative impact on the crystalline region of cellulose.

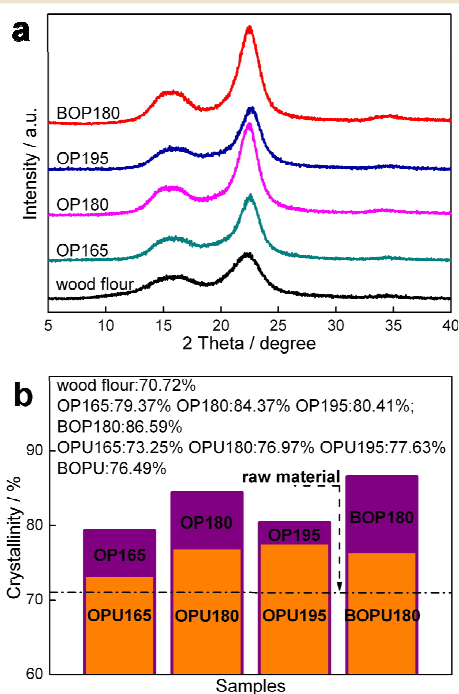


Fig. 5 (a) XRD patterns and (b) crystallinity of the pretreated samples and the obtained CNCs.

Green Chemistry ARTICLE

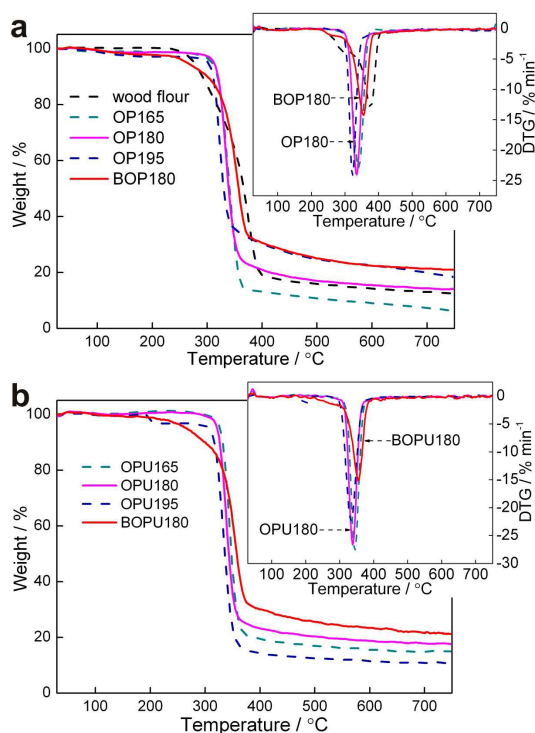


Fig. 6 TG curves of the (a) pretreated samples and (b) CNCs. The insets show the DTG curves.

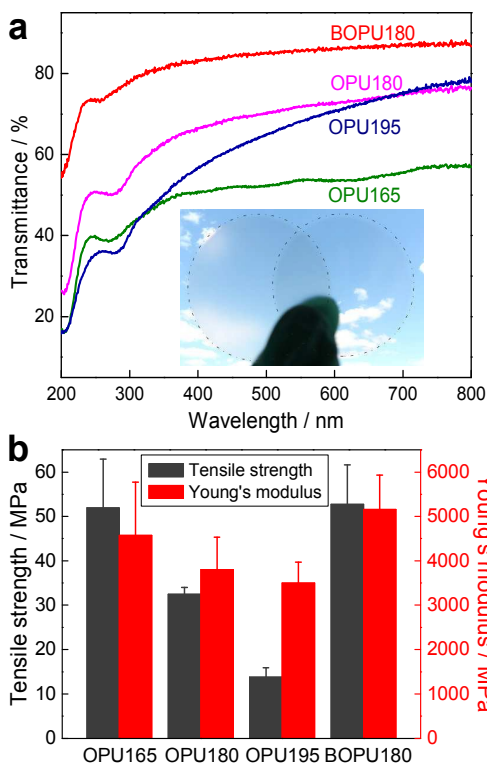


Fig. 7 (a) UV-vis transmittance spectra of the CNC nanofilms. The inset shows the photographs of OPU180 (left) and BOPU180 (right) nanofilms. (b) Ultimate tensile strength and Young's modulus of the CNC nanofilms.

Structure and properties of the CNC nanofilms

The assembly of CNCs are mainly determined by their morphologies and surface properties, as well as the drying process.^{39, 42–44} Drying by suction filtration and solvent evaporation of the CNC suspensions resulted in nanofilms. The average thickness of the nanofilms was 20–30 μm . Because of the dense packing of the CNCs, the nanofilms exhibited transparency (Fig. 7a). For the OPU165 nanofilm, some residual hemicellulose and cytoderm fragments remained (Fig. 8a), which caused surface roughness, and consequently the light transmittance was reduced. The nanofilms composed of OPU180, OPU195, and BOPU180 showed fine smooth morphology, and accordingly had good transparency (Fig. 8b, c and d). Particularly, through the comprehensive comparison of transmittance and mechanical properties, the BOPU180 nanofilm showed the highest optical light transmittance of 86% at 600 nm, equivalent to reported cellulose-based composite films with high transparency.⁴⁵ It also showed good mechanical properties with an ideal tensile strength > 50 MPa and Young's modulus > 5 GPa (Fig. 7b). All these factors make it a suitable candidate for application in displays, biosensors, and portable electron devices.

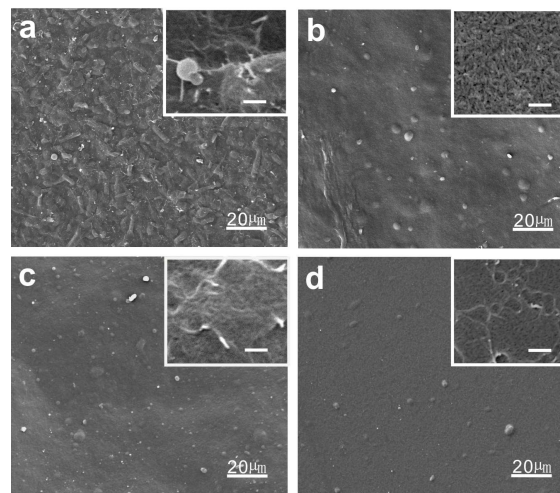


Fig. 8 SEM images of the nanofilms composed by (a) OPU165, (b) OPU180, (c) OPU195 and (d) BOPU180. The scale bar in all insets is 500 nm.

Conclusions

This study demonstrated a high delignification and fractionation efficiency of lignocellulose biomass by one-step treatment using ethanosolv, or two-step treatment using ethanosolv and peroxide to obtain high purity cellulose material. The ethanol solvothermal treatment can fractionate 97% of total lignin and 70% of the hemicellulose, and the subsequent treatment with peroxide can remove the rest lignin and one-third of the remanent hemicellulose. Consequently, high purity (95%) cellulose was successfully obtained to facilitate the ultrasonic processing to produce CNC. The resultant CNCs were 1–9 nm wide and within 500 nm long, with aspect ratios ranging from 10 to 150. They also showed high crystallinity and high thermal stability than those prepared by traditional methods. Consequently, the presented approach would facilitate the green

ARTICLE

Green Chemistry

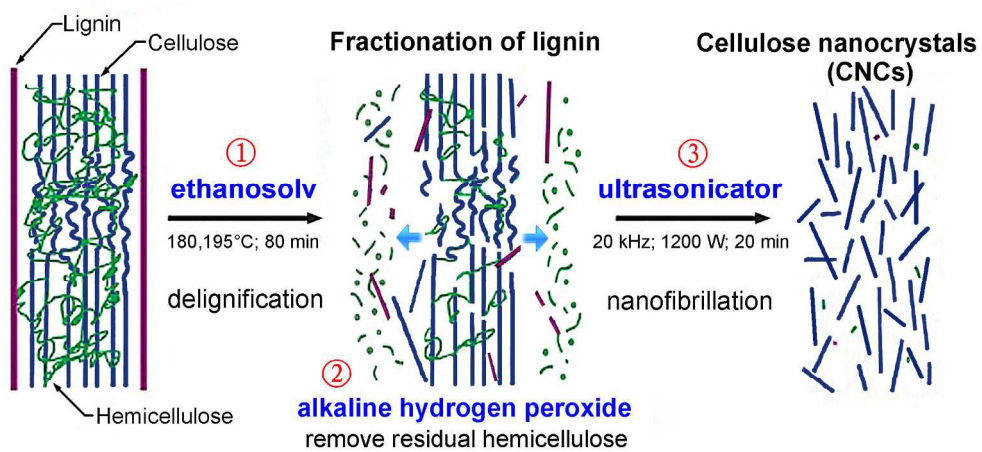
and facile utilization of lignocellulose, while not influencing the yield, morphology, crystallinity, and thermostability of CNC.

Acknowledgements

This work is financially supported by the National High-Level Personnel of Special Support Program, and in part by the National Natural Science Foundation of China (No. 31400495).

Notes and references

- 1 A. Dufresne, *Mater. Today*, 2013, **16**, 220.
- 2 C. Chatterjee, F. Pong and A. Sen, *Green Chem.*, 2015, **17**, 40.
- 3 R. J. Moon, A. Martini, J. Nairn, J. Simonsen and J. Youngblood, *Chem. Soc. Rev.*, 2011, **40**, 3941.
- 4 Y. H. Jung, T. H. Chang, H. Zhang, C. Yao, Q. Zheng, V. W. Yang, et al., *Nat. Commun.*, 2015, **6**, 7170.
- 5 T. Lu, Q. Li, W. Chen and H. Yu, *Compos. Sci. Technol.*, 2014, **94**, 132.
- 6 J. Gao, Q. Li, W. Chen, Y. Liu and H. Yu, *ChemPlusChem*, 2014, **79**, 725.
- 7 H. Yu, P. Chen, W. Chen and Y. Liu, *Cellulose*, 2014, **21**, 1757.
- 8 W. Gindl-Altmutter, M. Obersriebnig, S. Veigel and F. Liebner, *ChemSusChem*, 2015, **8**, 87.
- 9 W. Chen, H. Yu, Y. Liu, P. Chen, M. Zhang and Y. Hai, *Carbohydr. Polym.*, 2011, **83**, 1804.
- 10 H. P. S. Abdul Khalil, Y. Davoudpour, M. Nazrul Islam, A. Mustapha, K. Sudesh, R. Dungan, et al., *Carbohydr. Polym.*, 2014, **99**, 649.
- 11 K. Abe, S. Iwamoto and H. Yano, *Biomacromolecules*, 2007, **8**, 3276.
- 12 V. B. Agbor, N. Cicek, R. Sparling, A. Berlin and D. B. Levin, *Biotechnol. Adv.*, 2011, **29**, 675.
- 13 M. Iakovlev, X. You, A. van Heiningen and H. Sixta, *Cellulose*, 2014, **21**, 1419.
- 14 D. Carpenter, T. L. Westover, S. Czernik and W. Jablonski, *Green Chem.*, 2014, **16**, 384.
- 15 B. Deepa, E. Abraham, N. Cordeiro, M. Mozetic, A. P. Mathew, K. Oksman, et al., *Cellulose*, 2015, **22**, 1075.
- 16 T. vom Stein, P. M. Grande, H. Kayser, F. Sibilla, W. Leitner and P. D. de María, *Green Chem.*, 2011, **13**, 1772.
- 17 S. Gandolfi, G. Ottolina, R. Consonni, S. Riva and I. Patel, *ChemSusChem*, 2014, **7**, 1991.
- 18 R. A. Sheldon, *Green Chem.*, 2014, **16**, 950.
- 19 D. M. Nascimento, J. S. Almeida, A. F. Dias, M. C. B. Figueirêdo, J. P. S. Morais, J. P. A. Feitosa, et al., *Carbohydr. Polym.*, 2014, **110**, 456.
- 20 W. J. J. Huijgen, J. H. Reith and H. den Uil, *Ind. Eng. Chem. Res.*, 2010, **49**, 10132.
- 21 L. Hu, Y. Luo, B. Cai, J. Li, D. Tong and C. Hu, *Green Chem.*, 2014, **16**, 3107.
- 22 J. L. Wen, S. L. Sun, T. Q. Yuan, F. Xu and R. C. Sun, *J. Agric. Food Chem.* 2013, **61**, 11067.
- 23 A. A. Shatalov and H. Pereira, *Ind. Crop. Prod.*, 2013, **43**, 623.
- 24 J. G. Li, H. J. Zhang, C. Duan, Y. S. Liu and Y. H. Ni, *Bioresour. Technol.*, 2015, **192**, 11.
- 25 W. Chen, H. Yu, Y. Liu, Y. Hai, M. Zhang and P. Chen, *Cellulose*, 2011, **18**, 433.
- 26 L. Segal, J. J. Creely, A. E. Martin Jr and C. M. Conrad, *Text Res J*, 1959, **29**, 786.
- 27 J. X. Sun, X. F. Sun, R. C. Sun and Y. Q. Su, *Carbohydr. Polym.*, 2004, **56**, 195.
- 28 B. Sun, Q. X. Hou, Z. H. Liu and Y. H. Ni, *Cellulose*, 2015, **22**, 1135.
- 29 B. Scholze and D. Meier, *J. Anal. Appl. Pyrol.*, 2001, **60**, 41.
- 30 J. J. Villaverde, J. Li, M. Ek, P. Ligerio and A. de Vega, *J. Agric. Food Chem.*, 2009, **57**, 6262.
- 31 Y. Miyagawa, H. Kamitakahara and T. Takano, *Holzforchung*, 2013, **67**, 629.
- 32 J. L. Wen, T. Q. Yuan, S. L. Sun, F. Xu, and R. C. Sun, *Green Chem.*, 2014, **16**, 181.
- 33 M. Balakshin, E. Capanema, H. Gracz, H. M. Chang and H. Jameel, *Planta*, 2011, **233**, 1097.
- 34 J. Rencoret, P. Prinsen, A. Gutiérrez, A. T. Martínez and J. C. del Río, *J. Agric. Food Chem.*, 2015, **63**, 603.
- 35 T. Q. Yuan, S. L. Sun, F. Xu, and R. C. Sun, *J. Agric. Food Chem.*, 2011, **59**, 10604.
- 36 F. Jiang and Y.-L. Hsieh, *Carbohydr. Polym.*, 2013, **95**, 32.
- 37 P. Lu and Y.-L. Hsieh, *Carbohydr. Polym.*, 2010, **82**, 329.
- 38 I. Santoni, E. Callone, A. Sandak, J. Sandak and S. Dirè, *Carbohydr. Polym.*, 2015, **117**, 710.
- 39 J. P. F. Lagerwall, C. Schütz, M. Salajkova, J. Noh, J. H. Park, G. Scalia and L. Bergström, *NPG Asia Mater.*, 2014, **6**, e80.
- 40 H. Kargarzadeh, I. Ahmad, I. Abdullah, A. Dufresne, S. Y. Zainudin and R. M. Sheltami, *Cellulose*, 2012, **19**, 855.
- 41 A. W. McKenzie, *Appita J.*, 1968, **22**, 82.
- 42 J. Han, C. Zhou, Y. Wu, F. Liu and Q. Wu, *Biomacromolecules*, 2013, **14**, 1529.
- 43 W. Chen, Q. Li, Y. Wang, X. Yi, J. Zeng, H. Yu, et al., *ChemSusChem*, 2014, **7**, 154.
- 44 E. Rojo, M. S. Peresin, W. W. Sampson, I. C. Hoeger, J. Vartiainen, J. Laine, et al., *Green Chem.*, 2015, **17**, 1853.
- 45 H. Yano, S. Sasaki, M. I. Shams, K. Abe and T. Date, *Adv. Optical Mater.*, 2014, **2**, 231.



191x92mm (300 x 300 DPI)